energies

MDPI

Article

Fast Torque Computation of Hysteresis Motors and Clutches Using Magneto-static Finite Element Simulation

Gianvito Gallicchio [1,*], Marco Palmieri [1], Mauro Di Nardo [2] and Francesco Cupertino [1]

[1] Department of Electrical Engineering and Information Technology, Politecnico di Bari, 70126 Bari, Italy
[2] Power Electronics and Machine Control Group, University of Nottingham, Nottingham NG7 2RD, UK
* Correspondence: gianvito.gallicchio@poliba.it

Received: 2 August 2019; Accepted: 23 August 2019; Published: 28 August 2019

Abstract: Hysteresis motor and clutches have several advantages, such as constant torque from zero to synchronous speed, low torque ripple, and low fabrication cost. Low efficiency and power factor are the main features that have limited the application of this type of electrical machine to few applications. Being a niche argument, little literature has addressed the problem of analytical and finite element (FE) modelling of hysteresis electrical machines. This paper first describes the most important contributions of the literature on the analytical and FE modelling of hysteresis motors and clutches and then proposes a method for the fast computation of its performance. The proposed procedure consists of two steps: first, a magneto-static FE simulation is performed considering the normal magnetization curve of the hysteresis material; then, the average torque is computed by a post-processing analysis. The proposed method is used to analyze a hysteresis clutch and the obtained results are compared with those achieved using a commercial finite element software that implements a vector hysteresis model.

Keywords: hysteresis motor; hysteresis clutch; finite element analysis (FEA); numerical models; torque computation

1. Introduction

In the last decade, the manufacturing industry has been experiencing a paradigm shift referred to as Industry 4.0. In this framework, electrical machines can be considered one of the key technologies for the transition to the fourth industrial revolution. One of the main research topics in this field is related to the performance improvement of industrial processes whether from a single component or systems perspective [1,2].

Among the main requirements of the electrical machines for industrial applications, it is worth noting a flat torque versus speed characteristic, low-noise levels, and robust mechanical configurations.

The hysteresis motor is an electrical machine whose torque production relies on the principle of magnetic hysteresis, as first pointed out by Steinmetz [3]. In fact, the drive torque is proportional to the hysteresis losses in the rotating part of the machine.

The motor structure is quite simple: it consists of a slotted stator similar to that adopted in standard induction machines, whereas a ring of hard, or semi-hard, ferromagnetic material constitutes the rotor. The absence of rare earth magnets reduces the material costs and overcomes the issues related to the neodymium price uncertainty. Moreover, since there are no windings on the rotor, the Joule losses are concentrated in the stator, so the heat extraction is more simple and the cooling system can be less complex and more cost-effective.

As pointed out in [4], hysteresis motors can be a viable solution also for high-speed applications due to their simple and robust rotor structure, as well as their rotor-dynamics features [5].

Regarding low-speed applications, thanks to their flat torque versus speed characteristic and high reliability, hysteresis motors and clutches can be a valid choice for industrial applications or other devices like gyroscopes, clocks, magnetic ribbons in recorders, or low-power precision equipment [6].

However, as Steinmetz pointed out, the major drawbacks of these machines are the poor values of efficiency and power factor, which make it difficult for them to compete with those of induction motors or permanent magnet synchronous motors.

Being a niche argument, few contributions in the literature address hysteresis motors and clutches. Different analytical approaches to study the hysteresis motor are proposed in [7–9]; however, these methods show limits due to the approximations in the representation of the hysteresis loop (e.g.; elliptical shape). Other studies, such as [10,11] proposed a numerical method based on finite element simulation and vector hysteresis model to compute the output torque of the hysteresis motor. Both studies presented an iterative method to calculate the torque, whose main drawback is the increased computational burden.

The goal of this paper is to propose a new method for the fast evaluation of the hysteresis torque based on a single magneto-static finite element simulation coupled to a simple hysteresis model. The torque is calculated starting from the normal magnetization curve of the material and the value of the coercive field; from this data, it is possible to quickly estimate the minor loops of the material without performing any iterations. The low computational cost of the proposed method makes it suitable to be implemented within an automated design procedure.

2. Working Principle

When an external magnetic field is applied to a ferromagnetic material, the latter becomes magnetized in the direction of the external field, following the magnetization curve, until the saturation value is reached. When the external field is removed, due to the hysteresis behavior, the material shows a residual magnetization which can be removed by applying a coercive field in the opposite direction. By incrementing the external field in this direction, the magnetization of the material reaches the negative saturation value. Starting to increase the external field again, the closed loop is obtained, as shown in Figure 1.

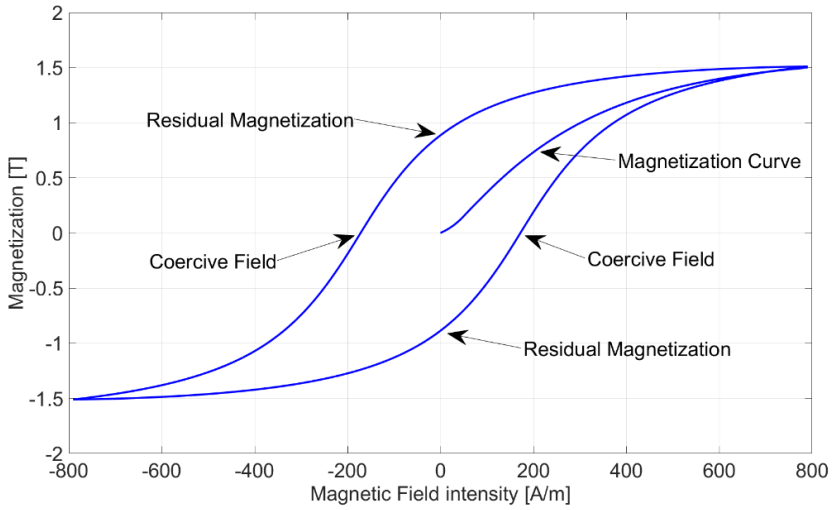

Figure 1. Typical hysteresis loop.

The hysteresis energy is proportional to the enclosed area of the loop; therefore, ferromagnetic materials can be classified as soft or hard according to the value of the coercive field as reported in Table 1.

Table 1. Classification of ferromagnetic material [12].

Type of Ferromagnetic Material	Coercive Field [A/m]
Soft	<1000
Semi-hard	<50,000
Hard	>50,000

While in classical electrical machine hysteresis is a negative phenomenon, in a hysteresis machine the torque is proportional to the hysteresis energy therefore hard or semi-hard ferromagnetic materials are used, so to improve the torque capability.

In Figure 2a it is presented a sketch of a typical hysteresis motor. The stator is slotted and the rotating parts are composed by a hard ferromagnetic ring. The coils are distributed in the stator slots to make a three-phase winding. The stator core is composed by a magnetic laminated steel whereas the rotor core could be magnetic or non-magnetic. The former is referred to as radial type machine, since the flux lines in the hysteresis ring will be mainly radial; in the latter case, the motor is called a circumferential machine, because the flux lines in the hysteresis ring will be mainly tangential.

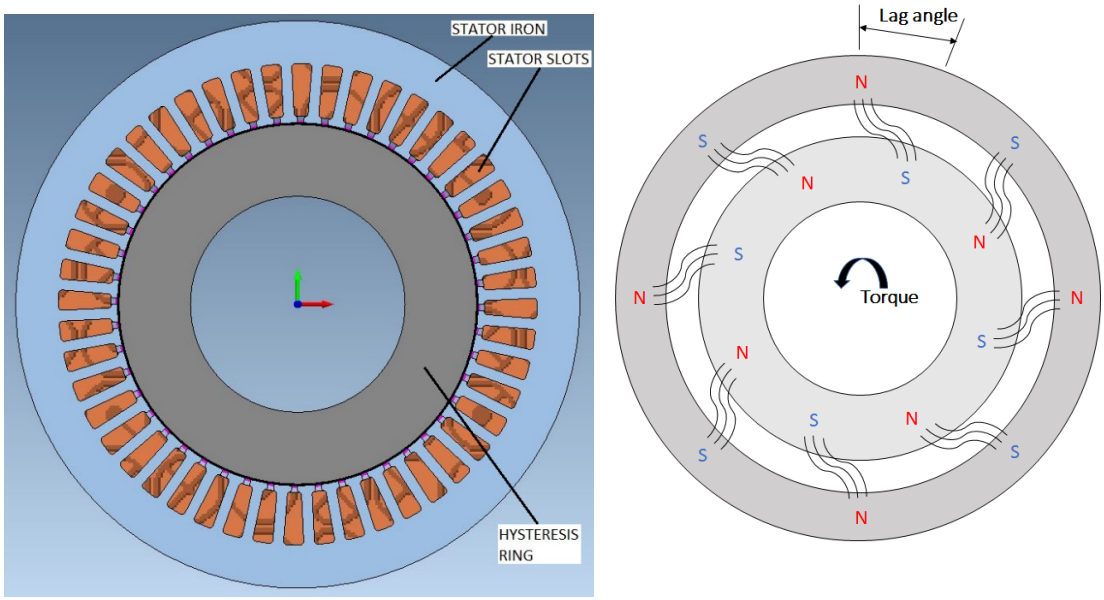

(**a**) (**b**)

Figure 2. (**a**) Typical Hysteresis motor; (**b**) torque production principle.

When the stator is fed by a set of 3 sinusoidal currents out of phase by 120 degrees, a rotating field is established at the airgap. Because of the hysteresis behavior, the flux density in the rotor material will lag behind the rotating field. This space angle between the rotating field and the flux density generates a torque [13]. From a qualitative point of view, the stator field creates poles on the rotor through magnetization and these poles follow the rotating field and pull the rotor along, as shown in Figure 2b. Neglecting hysteresis, the cycle of magnetization and demagnetization would be a reversible process. Conversely, due to hysteresis, the magnetized region tries to remain magnetized by following the stator field; thus, the rotor is pulled along by the poles [14]. The torque will be proportional to the hysteresis losses in the ring.

As pointed out in [15] the synchronous pull-out torque is expressed by Equation (1).

$$T = \frac{pV}{2\pi} \oint BdH \tag{1}$$

where p is the number of pole pairs, V is the volume of the hysteresis region and $\oint BdH$ is the area of hysteresis loop. This torque is the maximum value that the motor or the clutch can transmit during synchronous operation. If the load torque is higher than this value, the motor (or the coupler) starts to slip and the motor (or the coupler) behaves as an asynchronous motor (or coupler). The value of the torque in the asynchronous operation mode is the same of the synchronous pullout value. So, the torque is independent of the speed.

Thus, the torque will be the same from 0 to the synchronous speed. At the synchronous speed, the torque will be load-dependent. In fact, hysteresis motor behaves as induction motor when the angular speed is less than the synchronous speed, and as a permanent magnet synchronous motor when the motor reaches the synchronous speed [9]. As pointed out by Roters [7], when the rotor is slipping with respect to the stator field, the magnetization axis of the rotor will lag behind the stator field by a constant angle, but it will slip with respect to the rotor; when the synchronous speed is reached, the rotor axis will become stationary with respect to the rotor but will continue to lag the stator axis by an angle that depends on the characteristics of the rotor material. At the synchronous speed, the rotor remains magnetized and behaves like a surface-mounted permanent magnet rotor, with the same number of poles as the stator. At this stage, if the load torque is less than the maximum one, the rotor will accelerate with respect the stator field until the hysteresis torque (which depends by the lag angle) will balance the load torque. If the load torque exceeds the maximum torque, the rotor will decelerate to a stop (in this case, sub-synchronous operation is resumed, and the hysteresis torque is constant).

Hysteresis clutches and motors share the same working principle. In the hysteresis clutch, the stator is replaced by an electromagnet or permanents magnets. When the ring where permanent magnets are located starts turning, a rotating field is established in the hysteresis ring and a drive torque is produced. Similarly to the hysteresis motor, the induced poles pull the rotor along until it reaches the synchronous speed.

3. Analytical Approach

One of the most important contributions to the hysteresis motor theory was presented by Teare [8]. In his paper, he derived the torque equation by using the virtual work method. The torque is composed by three contributions: the radial one, the tangential one and the axial one. Generally, the axial component is negligible. Moreover, assuming a sinusoidal revolving magnetomotive force and supposing a large airgap reluctance with respect to the rotor one, the flux density in the rotor will be tangential and independent of the radius. So, the torque equation becomes:

$$T = K \oint B_\vartheta dH_\vartheta \tag{2}$$

where K is a constant related to the particular motor.

However, the actual flux density depends on the radius: it decreases moving from the airgap to the rotor core. This fact is less significative if the rotor core is non-magnetic and the radial thickness of the hysteresis ring is thin.

In 1963, Copeland and Slemon [9] proposed an analytical approach to study the performance of the motor, considering an idealized machine. They developed an equivalent circuit of the machine. The hysteresis loops (i.e., major and minor loops) are shaped in the form of parallelograms of constant width equal to twice the coercive force. However, the study was based on several assumptions: the dependence of the coercive force by the saturation level is not modeled; if the rotor is composed by hard ferromagnetic material, this assumption is very strong because the coercive force is sensitive to the variation of the saturation level. Moreover, the analysis is performed considering a high number of stator slots with sinusoidally distributed windings and the permeability of both stator iron and rotor core is infinite. The model, however, can be used for a first computation of the performance of the machine, provided that a more accurate evaluation requires a Finite Element Analysis (FEA). In Table 2 is reported a comparison between the analytical methods.

Table 2. Comparison between analytical approaches (+ worst, +++ best).

Analytical Approach	Hysteresis Loop Shape	Dependence of the Coercive Field by the Saturation Level	Type of Machine	Accuracy
[8]	Inclined ellipse	Yes	Circumferential	++
[9]	Parallelogram	No	Radial	+

4. Finite Element Analysis

Finite element analysis of a hysteresis motor is not a simple task. Generally, the hysteresis torque is not computed by FEA software because magnetic materials are usually modeled only by the normal magnetization curve. Hysteresis losses are computed in post-processing by using Steinmetz equations for laminated steels. Hysteresis behavior is not considered in the FEA analysis, therefore the hysteresis torque is not computed directly and a post-processing hysteresis model is often required.

4.1. Hysteresis Modeling

Most of the studies use a vector hysteresis model associated with FEA to calculate the hysteresis torque. Usually, the Jiles–Atherton model [16] or Preisach model [17] are adopted. The first model adopts the following equation for the numerical determination of hysteresis parameters:

$$\frac{dM}{dH} = (1-c)\frac{M_{an} - M_{irr}}{k\delta - \alpha(M_{an} - M_{irr})} + c\frac{dM_{an}}{dH} \tag{3}$$

where M_{irr} is the irreversible magnetization, M_{an} is the anhysteretic magnetization, δ is a directional parameter having the value +1 or –1, c is a parameter which represents reversible wall motion, H is the actual applied field and k is a parameter which determines the hysteresis loss. The paper describes a method to calculate the parameters to construct the hysteresis model. The procedure is iterative because the model is described by non-linear equations.

As reported in [18,19], classical Preisach Models have been applied to describe the hysteresis phenomenon. The model computes the magnetization M by convolving an input-dependent function $D(x, y)$ and a material-dependent Preisach function $P(x, y)$, by the Equation (4).

$$M = \iint D(x,y)P(x,y)dxdy \; If \; x \geq y \tag{4}$$

However, both Jiles–Atherton model and Preisach require accurate measurements of the complete major hysteresis loop, which is a non-trivial task when hard magnetic materials are considered.

A simpler method, based on the data available from the manufacturers, is reported in [20]. The presented algorithm needs the knowledge of the normal magnetization curve, the value of the intrinsic coercive field and, optionally, the value of the residual flux density. From the normal magnetization curve, the anhysteretic curve is obtained. Because the value of the intrinsic coercive field is known, it is possible to obtain the ascending and the descending branches of the major hysteresis loop, by solving a set of equations presented in [20]. To construct the minor loops, normal magnetization curve (which is the locus of the maxima of the minor loops) is used, combined with another set of equations. Moreover, the output of the model can be used to identify the parameters of a classic Preisach Model or to identify the parameters of a play model [21].

4.2. Fea Approach

In [10] it is proposed an iterative algorithm: in the first step, the elements of the rotor material present an arbitrary permeability and the finite element formulation can be derived, for example, from Equation (5):

$$B = \mu_d H + B_r \tag{5}$$

where μ_d is the differential permeability and B_r is the remanence.

Then, a finite element simulation is run. From FEA, the flux density for each ring element can be obtained. The maximum value of the tangential component of the flux density (B_{tan}) is the input for the hysteresis model. From the hysteresis model, it is possible to calculate the value of the field intensity (H) for each ring element. The new values of B_r and μ_d can be now computed. The procedure will continue until a convergence criterion is reached. This simulation results showed a good agreement with the experimental ones and the iterative method showed a good convergence. However, the iterative procedure is not simple. For every step, the hysteresis region must be divided into many elements, each of which has a certain permeability.

The procedure can be summarized as follows:

- Finite element analysis with initial permeability and initial B_r.
- Calculation of B_{tan} for each ring element and evaluation of the maximum of B_{tan}.
- Evaluation of the actual value of H from the hysteresis model.
- Computation of the new inputs for the finite element analysis.

Reza Nasiri-Zarandi and Mojtaba Mirsalim proposed another method to analyze hysteresis motor, based on a complex permeability concept [11]. They started from the measured hysteresis loops and extrapolated the normal magnetization curve by connecting the maxima of the measured hysteresis loops. The normal magnetization curve is the input for a magneto-static simulation. From magneto-static simulation an inclined ellipse is extracted based on (6) and (7):

$$\mu_r = \frac{B_{max}}{\mu_0 H_{max}} \tag{6}$$

$$\gamma = \arcsin\left(\frac{H_c}{H_{max}}\right) \tag{7}$$

These parameters are now imported in a steady-state solver. Then, the new values of B_{max} and H_{max} are calculated and so μ_r and γ. These new parameters are the new inputs for the steady-state simulation [11]. The procedure ends when a predefined convergence criterion is reached.

This method is simpler than the previous one because there is no Preisach Model or Jiles–Atherton Model, but, as pointed out by the authors, the computational cost is higher.

A similar approach is presented by Repetto and Uzunov [22]. In their paper, they made a magneto-static simulation using the normal magnetization curve to characterize the rotor material. Then, the first harmonic component of the magneto-motive waveform at rotor surface is extracted and given as an input to a hysteretic solution, limited to the rotor domain. The problem is then solved in terms of Cell Method, which is a scalar static hysteresis model.

In Table 3 is shown a comparison between the methods. The accuracy of the methods depends both on the number of assumptions and the agreement with the experimental results.

Table 3. Comparison between methods (+ worst, +++ best).

Method	Accuracy of the Model	Computational Cost	Ease of Implementation
[10]	++	+++	+++
[11]	+	+	+
[22]	+	+	+

5. Proposed Method

In order to reduce the computational cost and simplify the evaluation of the average torque of a hysteresis machine, this paper proposes a method which does not consider iterative algorithms or complex vector hysteresis models. The input data are the normal magnetization curve and the value of the coercive field.

In the first step, a magneto-static FEA is performed using the opensource software FEMM [23]. Only one magneto-static simulation is required, and it lasts at most 20 s. Then, the hysteresis region is discretized along the radial direction; the maximum value of the circumferential and radial components of the flux density, B_{tan} and B_{rad}, for each discrete radius of the hysteresis region is evaluated and stored. In fact, the value of B for each element calculated at a fixed radius does not change because each element will reach the same saturation level, during an electrical revolution of the magnetic field. Each maximum value of the flux density and the corresponding value of the magnetic field intensity are the input for a hysteresis model and are used to create the corresponding minor loop. The shape of these minor loops is related to the actual value of the coercive field, which depends on the saturation level. The coercive field for each value of maximum flux density is evaluated, according to equations presented in [20], as (8):

$$\text{if } H > H_{\mu max} H_{ci} = H_{tan} + \frac{H - H_{\mu max}}{H_{sat} - H_{\mu max}} (H_c - H_{tan}) \text{if } H < H_{\mu max} H_{ci} = H + \frac{H_{sat} - H}{H_{sat} - H_{res}} H_{res} \quad (8)$$

where H is the value of the magnetic field intensity derived from the magnetostatic simulation, H_{tan} is the intercept of the tangential line at the point of maximum permeability of the normal magnetization curve, $H_{\mu max}$ is the value of H at the point of maximum permeability, H_c is the coercive field at the maximum saturation level, H_{sat} is the maximum value of H and H_{res} is the value of in the $H_{an} - H$ plane, where H_{an} is the value of H in the anhysteresic curve, as shown in Figure 3. The blue curve is the anysteretic curve and represents the relationship between the values of B in the curve MTS and H_{an}. B_{MTS} has the expression presented in Equation (9), while H_{an} can be calculated by Equation (10).

$$\text{If } H < H_{\mu max} B_{MT} = \mu_{max} \cdot \left(H_{MT} - H_{\mu max} \right) + B_{\mu max} \text{If } H > H_{\mu max} B_{TS} = f(H_{TS}) \quad (9)$$

$$H_{an} = H_{MTS} - \Delta H \Delta H = H_{tan} \frac{H_{sat} - H_{MTS}}{H_{sat} - H_{tan}} \quad (10)$$

where H_{MT} is an array with linearly spaced values, H_{TS} is an array of H values extrapolated from the normal magnetization curve going from T to S, B_{TS} is an array of B values extrapolated from the normal magnetization curve going from T to S and H_{MTS} is obtained concatenating H_{MT} and H_{TS}. Starting from the actual value of H_{ci} and finding the analytical relantionship between B_{MTS} and H_{an} it is possible to construct the corresponding minor loop and, if $H_{ci} = H_c$, the major loop, creating a smooth curve passing through the points (H_{ci}, 0), (H_p, B_p), (-H_{ci}, 0) and (-H_p,-B_p), as shown in Figure 4.

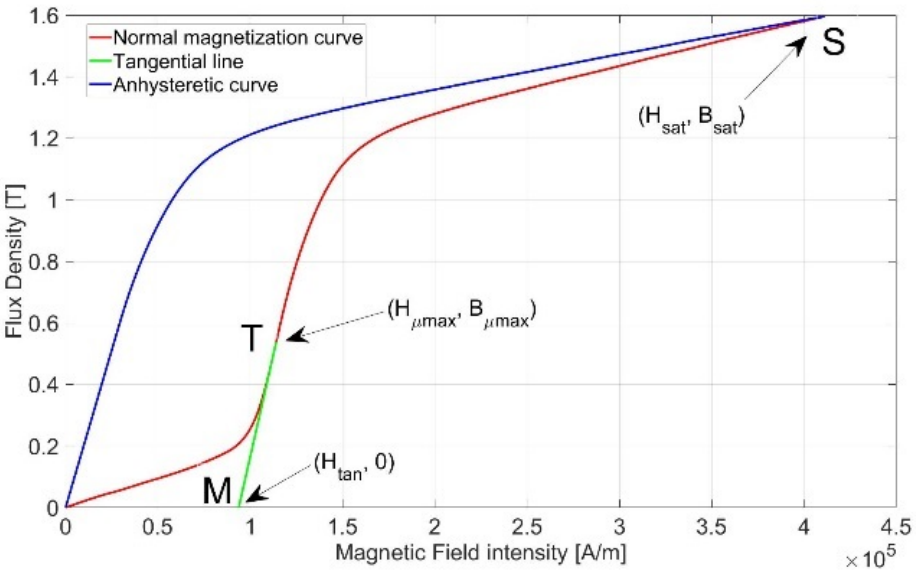

Figure 3. Tangential line and Anhysteretic curve.

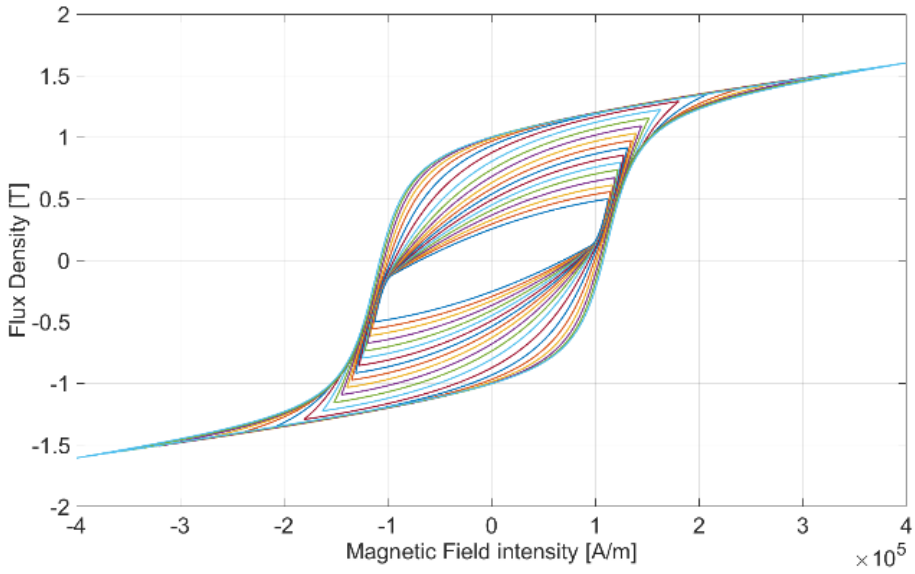

Figure 4. Minor loops construction.

In Figure 5 is shown a comparison between the measured major loops (the intrinsic one and the normal one) and the constructed major loops (the intrinsic one and the normal one) for AlNiCo 9. It can be noted that the hysteresis model shows a good agreement with the experimental data. This can be considered a further validation of the proposed method.

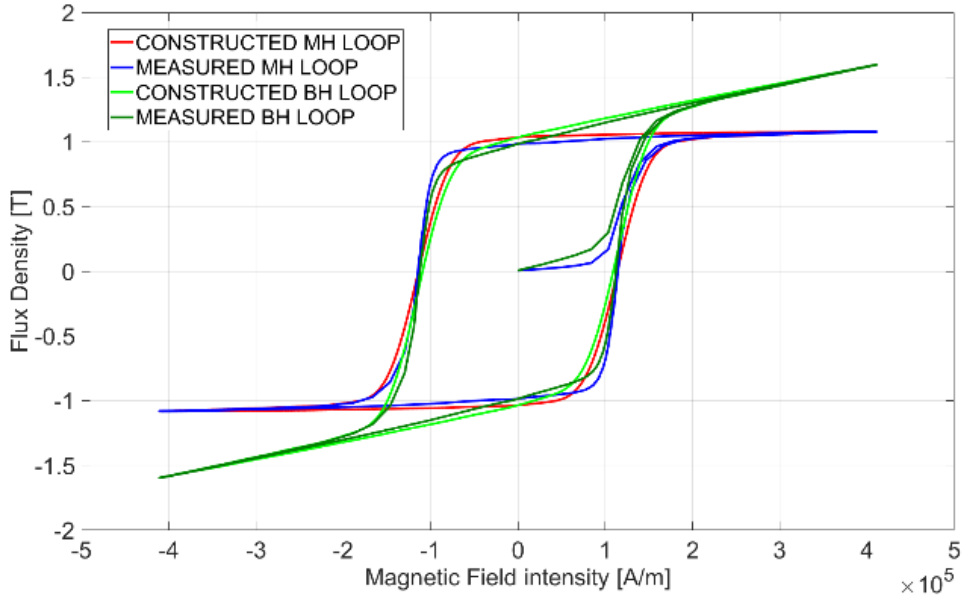

Figure 5. Comparison between constructed and measured hysteresis loop.

For each value of B_{rad} and B_{tan} extracted from the magneto-static simulation, the area of the corresponding hysteresis loop is computed. If the machine is circumferential or radial and the thickness of the hysteresis region is small, it is possible to evaluate the torque considering the maximum value of the flux density, because, in these cases, the peak value of the flux density does not change with the radius. In this way, the torque can be computed considering only one hysteresis loop and the whole volume of the hysteresis region. Otherwise, it is necessary to calculate the hysteresis energy for each component, radial and circumferential, by Equation (11):

$$E_{rad} = \sum_{k=1}^{N} A_{rad}(k) \cdot 2\pi \cdot r(k) \cdot \frac{(r(N) - r(1))}{N} E_{tan} = \sum_{k=1}^{N} A_{tan}(k) \cdot 2\pi \cdot r(k) \cdot \frac{(r(N) - r(1))}{N} \quad (11)$$

where $r(k)$ is the current radius of the hysteresis region, N is the number of the considered radii, $A_{rad}(k)$ and $A_{tan}(k)$ are the areas of the hysteresis loops corresponding to the radial and circumferential components of the flux density for a certain radius k, and $\frac{(r(N)-r(1))}{N}$ is Δr. A higher value of N will provide a better approximation for the integral expressed by Equation (12):

$$E_{rad} = \int_{r_1}^{r_2} A_{rad}(r) \cdot 2\pi \cdot r \cdot dr E_{tan} = \int_{r_1}^{r_2} A_{tan}(r) \cdot 2\pi \cdot r \cdot dr \quad (12)$$

then, the torque is calculated by Equation (13):

$$T = \frac{p}{2\pi} \cdot E \quad (13)$$

where p is the number of pole pairs of the machine and E is the sum of E_{rad} and E_{tan}.

If the hysteresis region is not a ring but is divided in a several numbers of bars, E must be modulated by the ratio between the actual volume of the hysteresis region and the volume of the ring considered in the Equation (11). The post-processing phase does not last more than 25 s. So, the complete computational time does not exceed 45 s. The quick evaluation of the torque will allow to use the proposed method within an automated design optimization procedure.

It is worth to note that the proposed method is valid if the hysteresis material is isotropic, without a preferential magnetization direction. The extension of the procedure to anisotropic materials is currently under investigation by the authors and it will be addressed in a future work.

Figure 6 shows the flowchart of the proposed method.

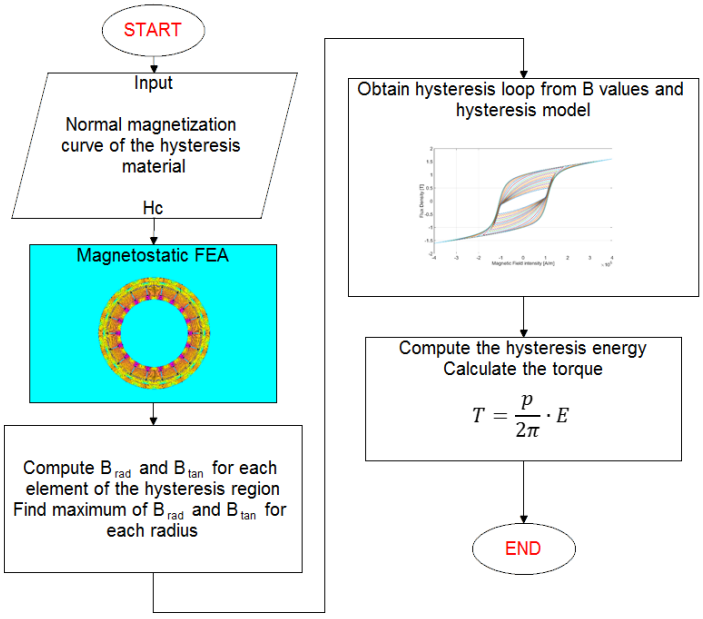

Figure 6. Flowchart of the proposed method.

6. Case of Study

The simulated machine is a hysteresis clutch with an inner ring composed of 18 NdFeB magnets and an outer ring composed of a hard ferromagnetic material (AlNiCo 9). The inner ring is the field generator and the outer ring is the hysteresis element. The inner and the outer cores are composed by solid magnetic steel (Figure 7). The main specifications of the machine are reported in Table 4.

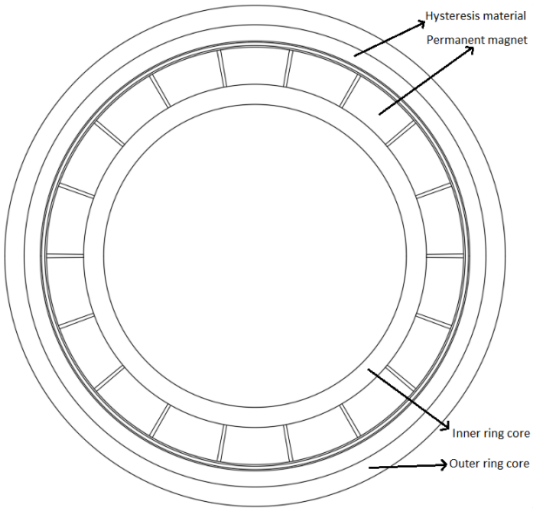

Figure 7. Hysteresis Clutch.

Table 4. Machine parameters.

Parameter	Value	Units
Number of pole pairs	9	\
Inner diameter	46.8	mm
Outer diameter	77.4	mm
Inner core radial thickness	3.1	mm
Outer core radial thickness	3	mm
Permanent Magnets radial thickness	5.75	mm
Hysteresis region radial thickness	2.5	mm
Axial length	27	mm

The major loop of the hysteresis material is reported in Figure 8a, whereas Figure 8b shows its normal magnetization curve implemented in the finite element formulation.

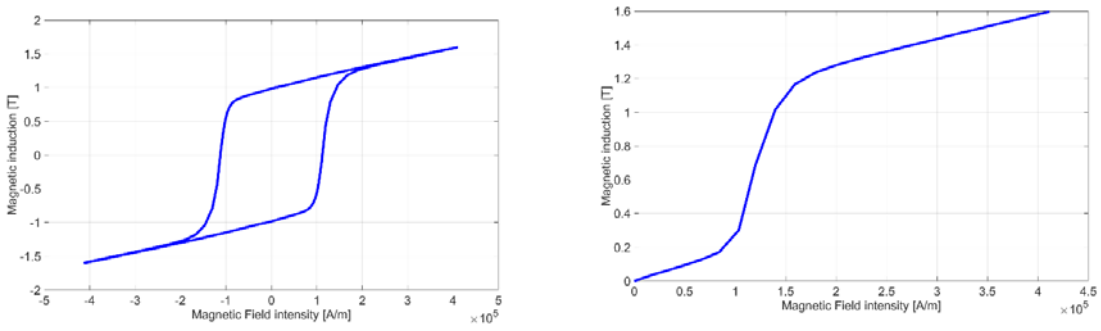

(**a**) (**b**)

Figure 8. (**a**) The major loop of the hysteresis material, (**b**) The normal magnetization curve implemented in the finite element formulation.

Figure 9 reports the flux density distribution obtained after the magneto-static analysis. The maximum value of B, computed in the hysteresis region, is 1.18 T which is lower than the saturation level (1.5 T). The value of B in the hysteresis material depends on the residual flux density of the magnets mounted on the inner ring. Using a magnet with a higher residual flux density, the hysteresis torque will be higher too. In Figure 10 are reported the hysteresis loops in the radial direction, whereas in Figure 11 are reported the hysteresis loops in the tangential direction, for various radii of the hysteresis region.

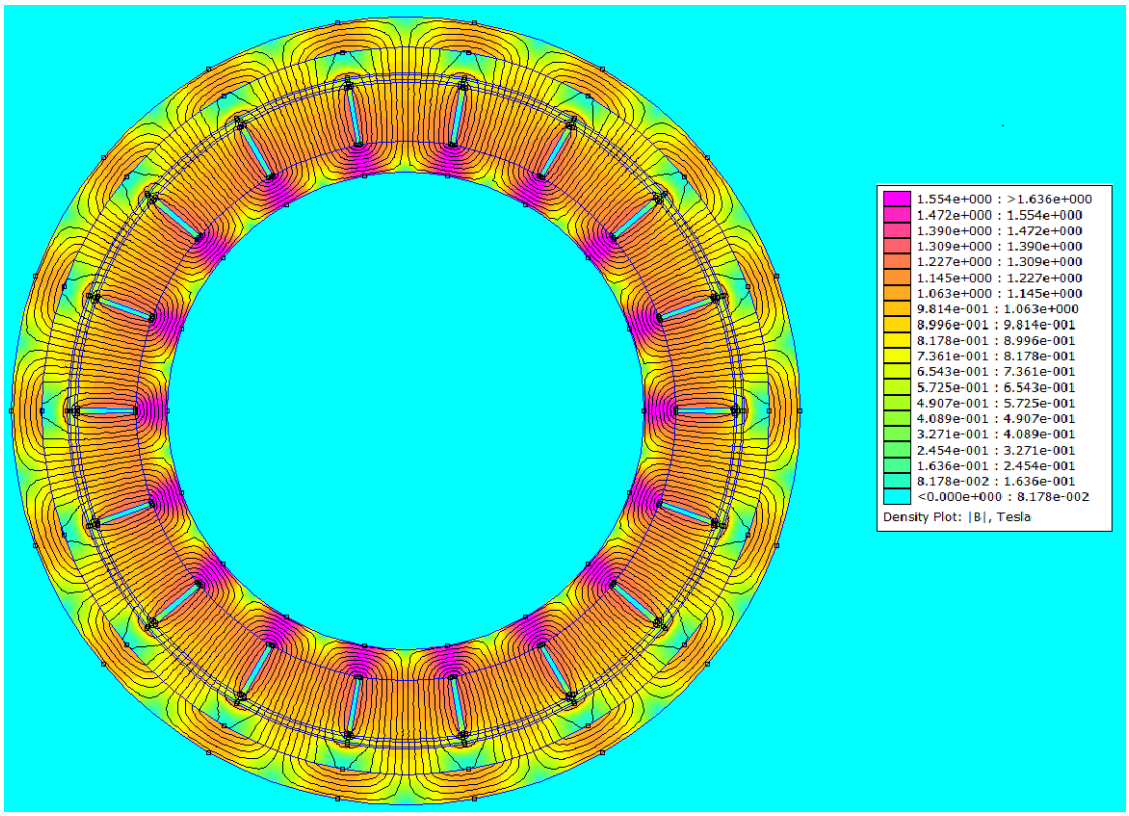

Figure 9. Flux density plot.

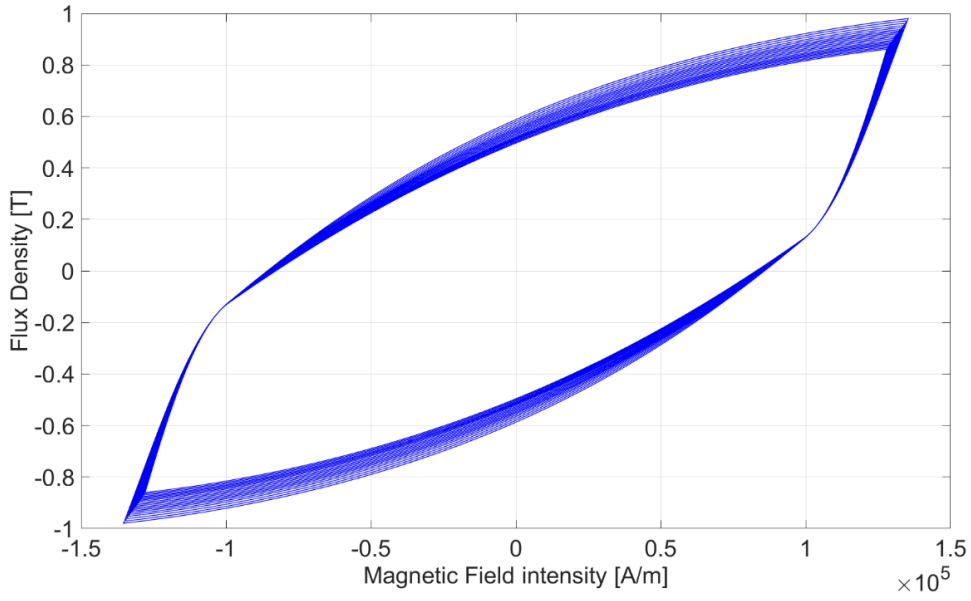

Figure 10. Radial hysteresis loops in the hysteresis region.

The computed torque is a mean value. The dynamic behavior of the machine is not considered in this kind of analysis. The torque derived from this model is compared with the mean torque extracted from a transient simulation performed with a commercial FE software (Ansys Maxwell) with the built-in vector hysteresis model presented in [20]. To the authors' knowledge, this software, used as a benchmark, is one of the few that implements a vector hysteresis model for hard magnetic material. The model of Ansys Maxwell requires:

1. the normal magnetization curve
2. the value of the intrinsic coercive field
3. the value of the residual flux density (optional)

The transient analysis is performed at locked outer ring, whereas the inner ring rotates at constant angular speed. As shown in Figure 12, at steady-state condition, the torque calculated from the commercial software is constant and its mean value is close to that computed by using the proposed procedure (as reported in Table 5).

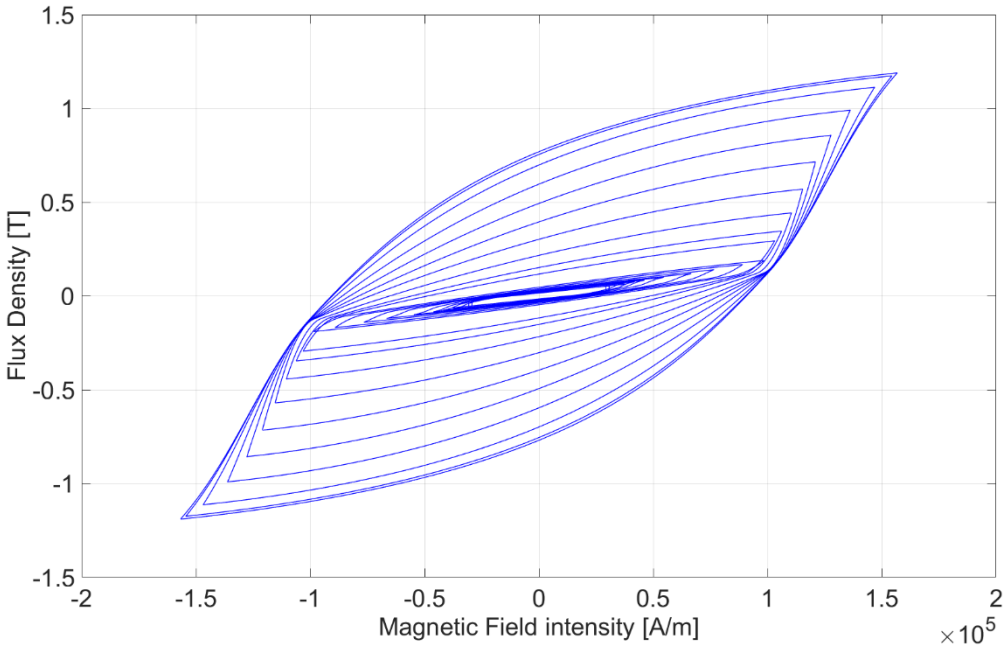

Figure 11. Tangential hysteresis loops in the hysteresis region.

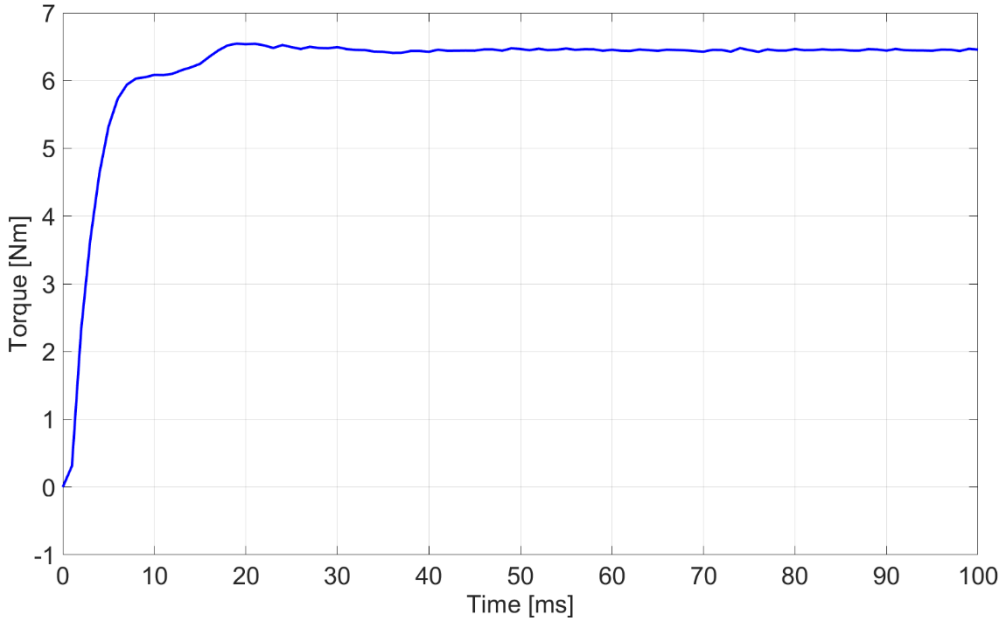

Figure 12. Torque vs time in a transient finite element analysis.

Table 5. Comparison between the methods.

Comparison Variable	Proposed Method	Transient Method
Mean torque [Nm]	6.48	6.45

7. Conclusions

This paper first describes the most important contributions of the up to date literature on the analytical and FE modelling of hysteresis electrical machine, highlighting the advantages and disadvantages of each method of analysis. In the second part of the paper, a method for the fast and easy computation of the average torque of a hysteresis motor or clutch is presented. The proposed method does not require the implementation of a vector hysteresis model, such as the Preisach model, Jiles Atherton model, or Play vector model. Its computational burden is reduced compared to the previously mentioned methods, and it allows the evaluation of the mean torque using an open-source FE software and an easy to implement post-processing analysis of the FE evaluated fields. The presented method has been compared with the one implemented in a commercial FE suit showing a really good agreement. A prototype of the hysteresis electrical machine is currently under manufacturing and it will be tested in order to validate the proposed method of analysis.

Author Contributions: The authors equally contributed to this article in terms of conceiving, theoretical analysis, numerical simulations, paper writing.

Funding: This work was supported in part by the project WindMill 4.0, code N7P89U5-INNONETWORK 2017, POR Puglia FESR- FSE 2014–2020.

Conflicts of Interest: The authors declare no conflict of interest.

References

1. Mayr, A.; Weigelt, M.; von Lindenfels, J.; Seefried, J.; Ziegler, M.; Mahr, A.; Urban, N.; Kühl, A.; Hüttel, F.; Franke, J. Electric Motor Production 4.0—Application Potentials of Industry 4.0 Technologies in the Manufacturing of Electric Motors. In Proceedings of the 8th International Electric Drives Production Conference (EDPC), Schweinfurt, Germany, 4–5 December 2018; pp. 1–13.
2. Tsai, W.-H. Green Production Planning and Control for the Textile Industry by Using Mathematical Programming and Industry 4.0 Techniques. *Energies* **2018**, *11*, 2072. [CrossRef]
3. Steinmetz, C.P. *Theory and Calculation of Alternating Current Phenomena*; McGraw Hill Book Company, Inc.: New York, NY, USA, 1908; p. 122.
4. Parvin, F.; Nasiri-Zarandi, R.; Mirsalim, M.; Cavagnino, A. General design algorithm for a hybrid hysteresis motor based on mathematical modeling. In Proceedings of the IECON 2016-42nd Annual Conference of the IEEE Industrial Electronics Society, Florence, Italy, 23–26 October 2016; pp. 1656–1661.
5. Circosta, S.; Galluzzi, R.; Bonfitto, A.; Castellanos, L.M.; Amati, N.; Tonoli, A. Modeling and Validation of the Radial Force Capability of Bearingless Hysteresis Drives. *Actuators* **2018**, *7*, 69. [CrossRef]
6. Galluzzi, R.; Amati, N.; Tonoli, A. Modeling, Design and Validation of Magnetic Hysteresis Motors. *IEEE Trans. Ind. Electron.* **2019**. [CrossRef]
7. Roters, H.C. The hysteresis motor-advances whick permit economical fractional horsepower ratings. *Trans. Am. Inst. Electr. Eng.* **1947**, *66*, 1419–1430. [CrossRef]
8. Teare, B.R. Theory of hysteresis-motor torque. *Electr. Eng.* **1940**, *59*, 907–912. [CrossRef]
9. Copeland, M.A.; Slemon, G.R. An analysis of the hysteresis motor I-analysis of the idealized machine. *IEEE Trans. Power Appar. Syst.* **1963**, *82*, 34–42. [CrossRef]
10. Kim, H.K.; Hong, S.K.; Jung, H.K. Analysis of hysteresis motor using finite element method and magnetization-dependent model. *IEEE Trans. Magn.* **2000**, *36*, 685–688.
11. Nasiri-Zarandi, R.; Mirsalim, M. Finite-element analysis of an axial flux hysteresis motor based on a complex permeability concept considering the saturation of the hysteresis loop. *IEEE Trans. Ind. Appl.* **2015**, *52*, 1390–1397.

12. Bi, S. Charakterisieren und modellieren der ferromagnetischen hysterese. Ph.D. Thesis, Friedrich-Alexander-Universität Erlangen-Nürnberg, Erlangen-Nürnberg, Germany, 2014.
13. Noh, M.; Gruber, W.; Trumper, D.L. Hysteresis Bearingless Slice Motors with Homopolar Flux-Biasing. *IEEE/ASME Trans. Mech.* **2017**, *22*, 2308–2318. [CrossRef] [PubMed]
14. Nitao, J.J.; Scharlemann, E.T.; Kirkendall, B.A. *Equivalent Circuit Modeling of Hysteresis Motors*; No. LLNL-TR-416493; Lawrence Livermore National Lab (LLNL): Livermore, CA, USA, 2009.
15. Canova, A.; Cavalli, F. Design procedure for hysteresis couplers. *IEEE Trans. Magn.* **2008**, *44*, 2381–2395. [CrossRef]
16. Jiles, D.C.; Thoelke, J.B.; Devine, M.K. Numerical determination of hysteresis parameters for the modeling of magnetic properties using the theory of ferromagnetic hysteresis. *IEEE Trans. Magn.* **1992**, *28*, 27–35. [CrossRef]
17. Bertotti, G. *Hysteresis in Magnetism: For Physicists, Materials Scientists, and Engineers*; Academic: New York, NY, USA, 1998; pp. 433–504.
18. Kim, H.S.; Hong, S.K.; Han, J.H.; Choi, D.J. Dynamic Modeling and Load Characteristics of Hysteresis Motor Using Preisach Model. In Proceedings of the 2018 21st International Conference on Electrical Machines and Systems (ICEMS), Jeju, Korea, 7–10 October 2018; pp. 560–563.
19. Torre, E.D. Existence of magnetization-dependent Preisach models. *IEEE Trans. Magn.* **1991**, *27*, 3697–3699. [CrossRef]
20. Lin, D.; Zhou, P.; Lu, C.; Chen, N.; Rosu, M. Construction of magnetic hysteresis loops and its applications in parameter identification for hysteresis models. In Proceedings of the 2014 International Conference on Electrical Machines (ICEM), Berlin, Germany, 2–5 September 2014; pp. 1050–1055.
21. Lin, D.; Zhou, P.; Bergqvist, A. Improved vector play model and parameter identification for magnetic hysteresis materials. *IEEE Trans. Magn.* **2014**, *50*, 357–360. [CrossRef]
22. Repetto, M.; Uzunov, P. Analysis of hysteresis motor starting torque using finite element method and scalar static hysteresis model. *IEEE Trans. Magn.* **2013**, *49*, 2405–2408. [CrossRef]
23. Finite Element Method Magnetics. Available online: http://www.femm.info (accessed on 3 July 2019).